

A spectroscopic study of a rich cluster at $z=1.52$ with Subaru & LBT: the environmental impacts on the mass-metallicity relation.

SHIGERU V. NAMIKI,^{1,2} YUSEI KOYAMA,^{1,2} MASAO HAYASHI,³ KEN-ICHI TADAKI,³ NOBUNARI KASHIKAWA,⁴ MASATO ONODERA,² RHYTHM SHIMAKAWA,² TADAYUKI KODAMA,⁵ ICHI TANAKA,² N. M. FÖRSTER SCHREIBER,⁶ JARON KURK,⁶ AND R. GENZEL^{6,7}

¹*Department of Astronomy, School of Science, Graduate University for Advanced Studies, Mitaka Tokyo 181-8588, Japan*

²*Subaru Telescope, National Astronomical Observatory of Japan, 650 North A'ohoku Place, Hilo, HI 96720, USA*

³*Optical and Infrared Astronomy Division, National Astronomical Observatory of Japan, Mitaka Tokyo 181-8588, Japan*

⁴*Department of Astronomy, School of Science, The University of Tokyo, 7-3-1 Hongo, Bunkyo-ku, Tokyo 113-0033, JAPAN*

⁵*Astronomical Institute, Tohoku University, 6-3 Aramaki, Aoba-ku Sendai, Japan 980-8578*

⁶*Max-Planck-Institut für extraterrestrische Physik (MPE), Giessenbachstr.1, D-85748 Garching, Germany*

⁷*Departments of Physics and Astronomy, University of California, Berkeley, CA 94720, USA*

(Received; Revised; Accepted April 30, 2019)

Submitted to ApJ

ABSTRACT

We present the results of our near-infrared (NIR) spectroscopic observations of a rich cluster candidate around a radio galaxy at $z = 1.52$ (4C65.22) with Subaru/MOIRCS and LBT/LUCI. We observed 71 galaxies mostly on the star-forming main sequence selected by our previous broad-band (photo- z) and narrow-band H α imaging observation in this cluster environment. We successfully confirmed the redshifts of 39 galaxies, and conclude that this is a gravitationally bound, real cluster at $z = 1.517$. Our spectroscopic data also suggest a hint of large-scale filaments or sheet-like three-dimensional structures crossing at the highest-density cluster core. By stacking the spectra to derive their average interstellar medium (ISM) gas-phase metallicity based on the [N II]/H α emission line flux ratio, we find that the mass-metallicity relation (MZR) in the 4C65.22 cluster environment is consistent with that of H α -selected field galaxies at similar redshifts. Our results suggest that the environmental impacts on the MZR is small at high redshifts, but a larger sample of high- z clusters and their member galaxies is still required to fully address the effect of environment as well as its cluster-cluster variation.

Keywords: galaxies: evolution, galaxies: ISM, galaxies: abundances, environment, spectroscopy

1. INTRODUCTION

Galaxy properties are characterized by a number of parameters such as e.g. stellar mass (M_*), star formation rate (SFR), color, or ISM gas-phase metallicity, and many studies have attempted to identify potential links between these parameters. A large sample of galaxies drawn by recent large surveys covering huge area on sky (like Sloan Digital Sky Survey; SDSS, York et al. 2000) allowed us to unveil many fundamental correlations between the physical parameters. One of the most prominent examples is the tight correlation between M_* and

SFR for star-forming galaxies; so-called star formation main sequence (SFMS; Brinchmann et al. 2004; Peng et al. 2010). The correlation between M_* and galaxy ISM gas-phase metallicity, which is often called mass-metallicity relation (MZR), is also well established in the local Universe (e.g. Tremonti et al. 2004).

The environment of galaxies is thought to be another important parameter which influences galaxy properties. In the local Universe, the central regions of galaxy clusters are in general dominated by red, passive galaxies, while blue, star-forming galaxies are mainly located in their outskirts (e.g. Dressler 1980; Goto et al. 2003; Gómez et al. 2003; Balogh et al. 2004; Tanaka et al. 2004). It is reported that the SFMS does not significantly change with environment in the local Universe

(Peng et al. 2010), and similarly, it is reported that MZR shows little environmental dependence at least in the local Universe (e.g. Cooper et al. 2008; Ellison et al. 2008; Wu et al. 2017).

However, the correlations between galaxy properties established in the local Universe are not necessarily applicable to galaxies in the distant Universe, where the cosmic star formation rate density is much higher than the present-day Universe (Hopkins & Beacom 2006). Our next important step is therefore to investigate the evolution of those relationships and understand how the correlations are formed and maintained across cosmic time and environment. Some authors have studied the evolution of the SFMS and/or MZR, and it is shown that the SFMS already exists at the very early epoch up to $z \sim 6$ (e.g. Salmon et al. 2015; Tomczak et al. 2016; Santini et al. 2017), and the MZR is also shown to exist up to $z \sim 3.5$ (e.g. Erb et al. 2006; Maiolino et al. 2008; Troncoso et al. 2014; Onodera et al. 2016; Sanders et al. 2018).

Considering the well-known, increasing fraction of star-forming galaxies in higher-redshift cluster environments (Butcher & Oemler 1984; van Dokkum et al. 2000), one might expect that environmental effects on galaxy properties could be weaker in the more distant Universe. However, it is always difficult to construct a large, uniform sample of galaxies in the distant Universe, and it prevents us from unveiling the environmental variation (if any) in the fundamental correlations between galaxy properties at high redshifts. Although some authors studied the environmental dependence of the SFMS by comparing star-forming galaxies in high- and low-density environment (e.g. Vulcani et al. 2010; Li et al. 2011; Koyama et al. 2013), a full consensus has not yet been obtained.

Furthermore, because ISM gas-phase metallicity measurement of distant galaxies requires a deep spectroscopy in NIR, it is much more difficult to investigate environmental dependence of MZR at high redshifts. There are only a limited number of observational studies discussing the environmental impacts on the MZR at the ‘‘cosmic noon’’ epoch (e.g. Kulas et al. 2013; Shimakawa et al. 2015; Valentino et al. 2015; Tran et al. 2015; Kacprzak et al. 2015; Maier et al. 2019), and interestingly, their conclusions are different from studies to studies. For instance, Kulas et al. (2013), Shimakawa et al. (2015), and Maier et al. (2019) investigated the ISM gas-phase metallicity of member galaxies of (proto-) clusters at $z = 1.5, 2.2, 2.3,$ and 2.5 . They suggested that the mean metallicity of low-mass cluster galaxies is *higher* than that of field galaxies with the same stellar mass. Kulas et al. (2013) and Shimakawa et al. (2015)

claimed that this difference can be explained by the metal recycling of momentum-driven outflow; i.e. outflow from a star-forming galaxy returns to itself in a short time scale due to the higher pressure of surrounding IGM in denser environment. This mechanism would work more effectively on low-mass galaxies because their escape velocity is lower than that of high-mass galaxies and thus metal-enriched gas is easier to be blown out from less massive galaxies. On the other hand, Tran et al. (2015) and Kacprzak et al. (2015) suggest that there is no significant environmental dependence in the MZR at $z \sim 2$. They concluded that the environmental effect is, if present, small and not a primary factor. In addition, Valentino et al. (2015) investigated a galaxy cluster at $z = 1.99$ and claimed that the member galaxies of this cluster have *lower* ISM gas-phase metallicity than field galaxies at the same redshift. Their interpretation is that the inflow of pristine gas into high-density environment would dilute the gas metallicity and enhance the specific SFR of galaxies residing in high-density environments.

In this paper, we present the results of our new spectroscopic observations for galaxies in another distant cluster at $z = 1.52$ (4C65.22). This cluster (candidate) was originally discovered by a photometric $H\alpha$ study of a radio galaxy field with Subaru (Koyama et al. 2014). They observed this region with broad-band and narrow-band ($H\alpha$) imaging with Subaru/MOIRCS (FoV: $7' \times 4'$, Ichikawa et al. 2006; Suzuki et al. 2008) and found 44 $H\alpha$ emitter candidates. In addition, by using the photometric redshifts (photo- z) derived with the optical (Subaru/Suprime-Cam; Miyazaki et al. 2002) and NIR (Subaru/MOIRCS) data, it was clearly shown that red-sequence galaxies (with $z' - J > 1.2$) are strongly clustered in the cluster central region ($\lesssim 200$ kpc), while blue galaxies ($z' - J < 1.2$) are located in its outskirts. They claimed that this is a good example of a ‘‘mature’’ cluster at this high redshift, although the cluster was not spectroscopically confirmed so far. We performed a follow-up NIR spectroscopy of star-forming galaxies in this rich cluster environment with Subaru/MOIRCS and Large binocular telescope (LBT)/LUCI. We first confirm the physical association of the cluster member galaxies in this field, and then we investigate the gas-phase metallicity (hereafter ‘‘metallicity’’ for simplicity) of those cluster member galaxies to discuss the environmental dependence of MZR at $z = 1.5$.

The structure of this paper is as the following. In Section 2, we show our sample selection and summarize the NIR spectroscopic observations with LBT/LUCI and Subaru/MOIRCS. In Section 3, we present the 2D dis-

tribution of cluster member galaxies and measure their gas-phase metallicity, and then discuss environmental dependence of MZR in Section 4. We summarize our results in Section 5. Throughout this paper, we adopt a flat Λ CDM cosmology with $\Omega_m = 0.3$, $\Omega_\Lambda = 0.7$ and $H_0 = 70 \text{ km s}^{-1} \text{ Mpc}^{-1}$, and a Salpeter initial mass function (IMF, Salpeter 1955). These cosmological parameters give a $1''$ scale of 8.46 kpc and the cosmic age of 4.2 Gyr at the redshift of our target cluster ($z = 1.52$). Magnitudes are all given in the AB system.

2. OBSERVATION & DATA

The aim of this study is to spectroscopically confirm the physical association of the strong over-density of galaxies in the 4C65.22 field reported by Koyama et al. (2014), and to study the properties of galaxies in high-density environment at this high redshift. We performed NIR spectroscopic observations of 71 galaxies in the 4C65.22 field with LBT/LUCI (Seifert et al. 2003) and Subaru/MOIRCS (Ichikawa et al. 2006; Suzuki et al. 2008). Our primary targets are $\text{H}\alpha$ emitters and blue galaxies (star-forming galaxy candidates) identified by Koyama et al. (2014), because it is much harder to detect continuum emission and absorption lines of red galaxies without emission lines at this redshift. In Fig.1, we show the distribution of our $\text{H}\alpha$ emitter sample on the M_* -SFR plane. The red circles represent $\text{H}\alpha$ -emitter candidates reported in Koyama et al. (2014), and the blue points indicate galaxies of which $\text{H}\alpha$ emission lines are detected by our spectroscopic observation. The histograms at the top and right-hand side show the normalized distribution of M_* and SFR of our sample, respectively. It can be seen that our spectroscopic samples are typical star-forming galaxies located on the SFMS at $z \sim 1.5$, and there is no strong bias with respect to the whole $\text{H}\alpha$ emitter sample in this field constructed by Koyama et al. (2014). Below, we describe the details of our observations.

2.1. LBT/LUCI spectroscopy

The NIR spectroscopic observation was carried out in May 2014 with LBT/LUCI; a NIR spectrograph and imager for LBT (Seifert et al. 2003). We used the multi-object slit (MOS) mode with 210_zJHK grating with $1''$ slit width, which gives a spectral resolution of $R \sim 3900$ over $\lambda = 1.55 - 1.74 \mu\text{m}$. We prepared 3 MOS masks, each of which includes 10 target galaxies. There are 3 galaxies observed with two masks, and the total number of our LUCI targets is 27. The exposure time for each configuration (LUCI-1, 2, and 3) is 70, 110, and 130 minutes, respectively, with a mean seeing size of $\sim 1''$. Table 1 summarizes our observation.

We reduced the data using a custom-made pipeline, Pyroscope (developed by J. Kurk). The pipeline process includes bad-pixels, cosmic ray correction, distortion correction, wavelength calibration for each slit, sky subtraction, and combine. With a visual inspection of the 2-D spectra, we identified pixels with emission lines and extracted the 1-D spectra. We detected emission line (with $> 3\sigma$) for 19 galaxies at $\lambda = 16370 - 16770 \text{ \AA}$. We note that this wavelength range corresponds to the transmission curve of NB1657 filter used in Koyama et al. (2014) to identify $\text{H}\alpha$ emitters at $z = 1.52$. For galaxies with emission lines, we determine the redshift of each galaxy by gaussian fitting with the weight determined by background noise spectrum. We also detect $[\text{N II}]\lambda 6583$ line for 12 out of 19 galaxies. For the remaining 7 galaxies (with single emission line detection), we cannot rule out the possibility that other emission lines at different redshifts (such as $[\text{O III}]\lambda 5007, \lambda 4959$ lines at $z \sim 2.3$ or $[\text{O II}]\lambda 3726, \lambda 3729$ lines at $z \sim 3$.) could contaminate. However, we believe that this is less likely; in the case of $[\text{O II}]\lambda 3726, \lambda 3729$ we could detect the doublets with the spectral resolution of LUCI, while in the case of $[\text{O III}]\lambda 5007, \lambda 4959$, we expect $\text{H}\beta\lambda 4861$ line (as well as $[\text{O III}]\lambda 4959$ line in the case of bright objects) within the observed wavelength range in addition to the $[\text{O III}]$ doublet. We therefore assume that the strong emission lines detected in the range of $\lambda = 16370 - 16770 \text{ \AA}$ are $\text{H}\alpha$, but much deeper spectroscopy would be needed to fully confirm their redshifts.

2.2. Subaru/MOIRCS spectroscopy

We also performed multi-object NIR spectroscopy of galaxies in the 4C65.22 field in May 2015 with Subaru/MOIRCS using zJ500 grism with $0.8''$ slit width which provides a spectral resolution of $R \sim 464$ over $\lambda = 0.9 - 1.78 \mu\text{m}$. We designed two MOS masks (with 33 objects for each), and the exposure time was 3 hours for each mask under the seeing conditions of $0.5'' - 0.8''$ (see also Table 1). We note that 16 of the MOIRCS targets are overlapped with our LUCI targets, so that the number of galaxies observed only with Subaru/MOIRCS is 41.

The data reduction was performed using the MOIRCS spectroscopic pipeline, MCSMDP (Yoshikawa et al. 2010). The pipeline process includes flat-fielding, bad-pixels, cosmic ray correction, distortion correction, wavelength calibration for each slit, sky subtraction, combine, and flux calibration. By inspecting the reduced spectra, we determined the redshifts of 17 galaxies (for which significant emission lines are detected) in the same way as described in Section 2.1. We note that, depending on the slit positions on the masks,

some of the spectra do not cover the wavelength range of $\lambda \sim 1.65 \mu\text{m}$ (where we expect the $\text{H}\alpha$ lines of cluster member galaxies). For those galaxies, we instead try to identify emission lines over the range between $\lambda = 12175\text{\AA}$ and 13015\AA to look for the $[\text{O III}]\lambda 5007$ line for the same redshift. With this approach, we additionally identify 3 galaxies in this field.

Table 1. Summary of our spectroscopic observations

Mask	Exp. time (min)	Seeing (arcsec)	Slit width (arcsec)	N_{obj}
LUCI-1	70	~ 1.0	1.0	10
LUCI-2	110	~ 0.7	1.0	10
LUCI-3	130	~ 1.2	1.0	10
MOIRCS-1	180	~ 0.5	0.8	33
MOIRCS-2	180	~ 0.8	0.8	33

2.3. Final Sample

We successfully determined the redshifts of 39 galaxies in total; 19 from LUCI, 27 from MOIRCS, and 7 are observed with both. For 7 galaxies observed with both LUCI and MOIRCS, we confirm that their redshifts derived from LUCI/MOIRCS data are consistent, suggesting no systematic bias between the data obtained with different telescopes/instruments. We show in Table 2 the full list of the spectroscopically confirmed cluster member galaxies in the 4C65.22 field and their basic properties.

We comment that we quote the M_* and SFR derived by Koyama et al. (2014); they determined M_* with K_s -band photometry with $M_*/L_{K_s,obs}$ correction based on the $z' - K_s$ color (see eq.1 in Koyama et al. 2014), while they derived SFR with $\text{H}\alpha$ photometry. To measure the $\text{H}\alpha$ flux of individual galaxies, they first calculated the $\text{H}\alpha + [\text{N II}]$ line flux, continuum flux density, and EW_{rest} of each $\text{H}\alpha$ emitter from their broad-band and narrow-band imaging data. They derived the $[\text{N II}]/\text{H}\alpha$ line flux ratio from the $\text{H}\alpha + [\text{N II}]$ equivalent width using the empirical relation for local star-forming galaxies established by Sobral et al. (2012). Then, they corrected for the dust attenuation effect with $\text{SFR}_{\text{H}\alpha}/\text{SFR}_{\text{UV}}$ ratio (Buat 2003; Tadaki et al. 2013; see also Koyama et al. 2014) to finally derive SFR and sSFR of the $\text{H}\alpha$ emitter sample. We note that the $[\text{N II}]$ correction and the dust extinction correction are the major sources of uncertainty when deriving the SFRs with this approach. Koyama et al. (2015) reported that the uncertainty associated with the dust extinction correction from the

$\text{H}\alpha/\text{UV}$ ratio is typically ~ 0.4 mag. Also, Villar et al. (2008) showed that the scatter around the correlation between the $\text{H}\alpha/[\text{N II}]$ ratio and the $\text{H}\alpha + [\text{N II}]$ equivalent width is ~ 0.4 dex. Accordingly, we estimate the typical error of the SFR of our sample is ~ 0.2 dex. On the other hand, for the stellar mass estimate, we simply propagate the photometric errors of our z -band and K_s -band data. These uncertainties are shown with the red-line error-bars in Fig.1.

We have mainly used $\text{H}\alpha$ line for the redshift determination, but another important goal of this study is to investigate the metallicity of galaxies in this cluster region. In order to use N2 index (Pettini & Pagel 2004) for metallicity calibration (see Sec.3.3), we choose galaxies whose $[\text{N II}]\lambda 6583$ emission line is not contaminated by strong OH night sky lines. We visually inspect the spectra of our final sample, and carefully select 19 galaxies from LUCI sample and 12 galaxies from MOIRCS sample, in which 5 galaxies are observed with both instruments.¹ We use these 26 ‘‘clean’’ galaxies when we study the environmental impacts on the MZR (Sec.3.3). Here we note that we do not apply any aperture correction, because the results of this paper rely only on the $\text{H}\alpha$ and $[\text{N II}]\lambda 6583$ line flux ratio. We note that the seeing size is larger than the slit width for 10 galaxies observed with LUCI-3. This slightly degrades the quality (S/N) of the spectra, but the line flux ratio should not be strongly affected.

Finally, we note that AGNs can contribute to enhance their $[\text{N II}]$ emission line fluxes, which might affect our metallicity measurement (N2 index, Pettini & Pagel 2004; see Sec.3.3). In addition, it is also expected that AGN at these redshifts are often accompanied by strong outflow (Genzel et al. 2014). Because the S/N ratio of our MOIRCS sample is not so high, we are not able to rule out the possibility of AGN. For galaxies observed with LUCI, we carefully inspected each spectrum, and we confirm that there is no broad-line features with e.g. $FWHM \gtrsim 1000$ km/s or no extremely enhanced $[\text{N II}]\lambda 6583$ emission lines in our sample. We therefore conclude that the effect from type-1 AGN is small, but we cannot eliminate the possibility of contamination from type-2 AGN. On the other hand, for the galaxies observed with MOIRCS, we examine the line flux ratios on the BPT diagram (e.g. Baldwin et al. 1981, Kewley et al. 2013) using the stacked spectrum

¹ We note that the FWHMs of OH emission lines are large for our MOIRCS spectra because of their spectral resolution (~ 290), and we realize that the relatively large number (15) of our MOIRCS sample are severely affected by the OH emission lines at the wavelengths corresponding to their $[\text{N II}]\lambda 6583$ lines.

(see Sec.3.2). We find that the emission line flux ratios for both high-mass ($10^{10.48} M_{\odot} < M_{*} < 10^{11.41} M_{\odot}$) and low-mass ($10^{9.93} M_{\odot} < M_{*} < 10^{10.48} M_{\odot}$) subsamples are consistent with HII (star-forming) galaxies on the BPT diagram at $z = 1.5$ (Kewley et al. 2013), but it is difficult to completely rule out the potential contribu-

tion from AGNs due to the large error in $\log([\text{O III}]/\text{H}\beta)$ (~ 0.3 dex)². We thus need to keep in mind that the metallicity derived for our sample may be slightly over-estimated by the potential AGN contribution.

Table 2. List of all H α detected sample

ID	R.A.	Dec.	Redshift	M _*	SFR	Instrument	Lines	Stacking
	(deg)	(deg)		$\log_{10}\left(\frac{M_{*}}{M_{\odot}}\right)$	$\log_{10}\left(\frac{\text{SFR}}{M_{\odot} \text{ yr}^{-1}}\right)$		L/M	
293	266.822007	65.514093	1.5135 \pm 0.0029	10.14 \pm 0.25	1.49	M	H α , [N II], [O III]	Y
357	266.767425	65.516084	1.5135 \pm 0.0031	10.75 \pm 0.05	1.47	M	H α , H β	Y
409	266.786743	65.517948	1.5130 \pm 0.0027	10.70 \pm 0.05	1.27	M	H α , [N II]	Y
453	266.73966	65.519072	1.5119 \pm 0.0026	–	–	M	H α , [O III]	–
538	266.79246	65.521753	1.5312 \pm 0.0381	–	–	M	H α	–
576*	266.705835	65.523181	1.4492 \pm 0.0021	11.06 \pm 0.02	1.21	M	H α	–
665*	266.73212	65.526527	1.6493 \pm 0.0039	–	–	M	H α	–
874	266.908468	65.535837	1.5133 \pm 0.0009	10.63 \pm 0.07	1.41	L	H α	Y
930	266.793808	65.537622	1.5104 \pm 0.0017	10.32 \pm 0.15	1.01	M	H α , [N II], [O III]	Y
1002	266.680192	65.540946	1.5139 \pm 0.0009	10.73 \pm 0.05	1.54	L	H α , ([N II])	Y
1006	266.821641	65.541230	1.5126 \pm 0.0006	10.45 \pm 0.09	1.09	L/M	H α , H β	Y
1046	266.811661	65.542944	1.4980 \pm 0.0017	11.38 \pm 0.02	1.51	M	H α	–
1085	266.773938	65.544516	1.5247 \pm 0.0009	10.30 \pm 0.18	1.57	L/M	H α , [N II]	Y
1151	266.808950	65.546952	1.5338 \pm 0.0013	10.78 \pm 0.04	1.49	L/M	H α , [N II]	Y
1193	266.857945	65.548677	1.5153 \pm 0.0007	10.21 \pm 0.16	1.26	L	H α	Y
1248	266.818480	65.550677	1.5157 \pm 0.0011	11.28 \pm 0.02	1.89	L	H α , ([N II])	Y
1249	266.823656	65.550228	1.5211 \pm 0.0007	10.87 \pm 0.05	1.68	L/M	H α , [N II], (H β)	Y
1259	266.910546	65.551014	1.5192 \pm 0.0003	11.32 \pm 0.01	1.70	L	H α , ([N II])	Y
1263	266.639261	65.550909	1.5130 \pm 0.0008	9.93 \pm 0.38	1.19	L	H α	Y
1271	266.737076	65.551622	1.5240 \pm 0.0027	10.65 \pm 0.06	0.71	M	H α , [N II], [O III], H β	Y
1292	266.876375	65.552945	1.5117 \pm 0.0014	11.41 \pm 0.02	2.19	L	H α , ([N II])	Y
1304	266.782085	65.552903	1.5180 \pm 0.0008	10.23 \pm 0.14	1.19	L/M	H α , ([N II])	Y
1328	266.76224	65.552301	1.5224 \pm 0.0036	–	–	M	H α	–
1339	266.848079	65.552234	1.5167 \pm 0.0008	10.10 \pm 0.25	1.41	L	H α , [N II]	Y
1369	266.810181	65.555050	1.5211 \pm 0.0007	9.93 \pm 0.21	0.80	L	H α , ([N II])	Y
1400	266.711057	65.556204	1.5150 \pm 0.0034	10.41 \pm 0.09	1.29	M	H α	Y
1412	266.803357	65.556741	1.5135 \pm 0.0030	10.70 \pm 0.05	1.20	M	H α , ([N II])	Y
1422*	266.713480	65.557074	1.5567 \pm 0.0018	11.45 \pm 0.01	–	M	H α	–

Table 2 continued

² The large errors for the $\log([\text{O III}]/\text{H}\beta)$ ratio are partly caused by the contamination from strong OH emission lines at the wavelengths of their H β and/or [O III] lines. We carefully removed the spectra whose H α or [N II] lines are contaminated by OH emission lines from our analyses (see also Sec.3.2), but we do not do this for the H β or [O III] lines to keep a reasonable sample size (and it is not a problem because we do not use H β or [O III] lines for the metallicity measurements in this study).

Table 2 (*continued*)

ID	R.A.	Dec.	Redshift	M_*	SFR	Instrument	Lines	Stacking
	(deg)	(deg)		$\log_{10} \left(\frac{M_*}{M_\odot} \right)$	$\log_{10} \left(\frac{\text{SFR}}{M_\odot \text{ yr}^{-1}} \right)$	L/M		Y/-
1456	266.722739	65.559353	$1.5124^{\pm 0.0017}$	$10.43^{\pm 0.09}$	1.25	L/M	H α , ([N II])	Y
1461	266.909417	65.559817	$1.5129^{\pm 0.0011}$	$10.85^{\pm 0.07}$	1.84	L	H α	Y
1500* [†]	266.86996	65.56176	$1.4523^{\pm 0.0019}$	–	–	M	[O III]	–
1509	266.736187	65.561929	$1.5232^{\pm 0.0008}$	$10.46^{\pm 0.09}$	1.65	L/M	H α , [O III], H β	Y
1521	266.644548	65.562259	$1.5126^{\pm 0.0008}$	$10.87^{\pm 0.03}$	1.87	L	H α , [N II]	Y
1554	266.682257	65.563721	$1.5154^{\pm 0.0004}$	$10.66^{\pm 0.07}$	1.89	L	H α	Y
1567 [†]	266.683695	65.564301	$1.5182^{\pm 0.0028}$	$11.00^{\pm 0.04}$	1.97	M	[O III], H β	–
1604* [†]	266.837147	65.565738	$1.4912^{\pm 0.0044}$	–	–	M	[O III]	–
1644*	266.73666	65.568059	$1.5180^{\pm 0.0026}$	–	–	M	H α , [O III]	–
1887	266.767721	65.573595	$1.5391^{\pm 0.0026}$	$10.38^{\pm 0.16}$	1.28	M	H α , (H β)	–

NOTE—We include marginal detection ($< 2\sigma$) in the column of "Lines" and they are surrounded by the parentheses. [O III] and H β lines are detected only for MOIRCS targets because of the wavelength coverage. There are 7 galaxies whose H α lines fall outside the range of NB1657 (marked as *). [†] means the objects identified only with [O III]. M_* and SFR are not shown for galaxies which were not detected at K-band or NB1657 in Koyama et al. (2014). "L" and "M" in the 'Instrument' column means galaxies observed with LUCI and MOIRCS, respectively. The errors in M_* are derived from the photometric uncertainties, while we assign a typical 0.2-dex errors in SFR for all the galaxies (see Sec.2.3).

3. RESULT

3.1. Redshift Distribution & 2D-map

We show in Fig.2 the redshift distribution of our spectroscopic sample. The blue and red histograms indicate the number of galaxies observed with LUCI and MOIRCS, respectively. The magenta histogram shows the galaxies observed with both LUCI and MOIRCS. We here use LUCI data for the galaxies observed by both LUCI and MOIRCS. The black solid-line curve drawn in Fig.2 is the average filter response function of the MOIRCS NB1657 filter at the center of the FoV, while the dotted-line curves are the transmission at the edge of FoV (Tanaka et al. 2011); we note that the response function of the MOIRCS NB1657 filter changes with the location within the FoV. It is now clear that z_{spec} of galaxies in the 4C65.22 field are concentrated at $z = 1.510 - 1.525$ with very few outliers. This range is much narrower than the width of the narrow-band filter (even if we take into account the wavelength shift of the filter transmission at the edge of the FoV), suggesting that these galaxies are in fact concentrated in this small redshift range and not randomly distributed.

In Fig.3, we show the 2-D distribution of our spectroscopic sample. The triangles, squares, and circles indicate galaxies with spec- z determined by LBT/LUCI, Subaru/MOIRCS, and both of the instruments, respectively. The top and right panels show the projected

distribution on the R.A.- z and Dec.- z plane, respectively. It can be seen that the relatively high- z data points tend to be located in the cluster central region (or high-density regions), while the low- z data points tend to be located in the outskirts, suggesting that there are two large-scale filaments (or planes) crossing at the central region of the cluster. Such complicated large-scale structures are often seen in the nearby Universe or in numerical simulations, and our data suggests that the situation seems to be similar around this newly discovered structure at $z = 1.52$.

To determine the redshift of the cluster by eliminating the effect of surrounding structures, we here focus on galaxies located in the very central region. By taking the median of the z_{spec} for galaxies located within 1 arcmin from the density peak (corresponding to 500 kpc, green circle in Fig. 3), we determine the redshift of this galaxy cluster to be $z = 1.517$. We note that there still remains an uncertainty for the estimate of the cluster redshift because 8 red passive galaxies dominating the very central region of the cluster are not observed in this study (see Koyama et al. 2014).

3.2. Stacking & Fitting

We will discuss the metallicity of the cluster member galaxies and their environmental dependence in the next section. However, the signal-to-noise ratios of our data are not very high (typically $S/N(\text{H}\alpha) \sim 4$), and it is impossible to determine the metallicity of individual galaxies. We therefore apply stacking analysis to derive aver-

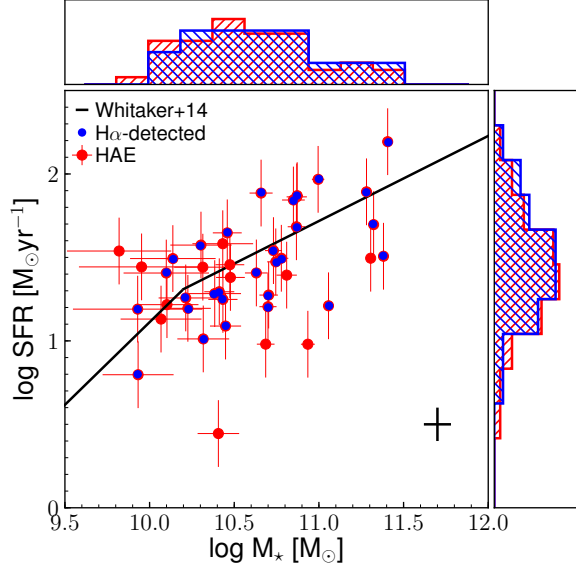


Figure 1. The distribution of our sample on the stellar mass versus star formation rate plane. The red circles show H α emitters (HAE) candidates selected in Koyama et al. (2014), and the blue points are HAEs confirmed by our spectroscopic observation. The black solid line indicates the star-forming main sequence at $z = 1.52$ (Whitaker et al. 2014). The errorbars for stellar mass are calculated from the photometric uncertainties in Koyama et al. (2014), while we adopt a typical uncertainty (~ 0.2 dex) in SFRs for all our sample (see 2.3). The histograms in the top and right panels show the normalized distribution of stellar mass and SFR of the HAEs (red) and our spectroscopic members (blue), respectively.

age metallicity for carefully selected 19 galaxies observed with LUCI and 12 galaxies observed with MOIRCS, whose H α and [N II] lines are not contaminated by strong OH sky lines (we note that this includes 5 galaxies observed with both LUCI and MOIRCS). Also, to study the stellar mass dependence of the metallicity of cluster galaxies, we divide our sample into two equal-sized bins by the median stellar mass (at $10^{10.48} M_{\odot}$, for LUCI and MOIRCS sample separately due to their different spectral resolution), and perform stacking analysis as described below for each subsample.

We first determine the continuum level of individual galaxies by applying the linear fitting to the spectrum around H α except for emission lines, and subtract it from the individual spectrum. We then normalize the spectra by their H α flux before stacking. We note that the details of the spectral stacking procedure are different from studies to studies. In particular, this flux normalization step is not performed in many studies. This step would not be necessary when we can assume that the galaxies used for stacking analysis have the same properties (e.g. in the case that the sample has same

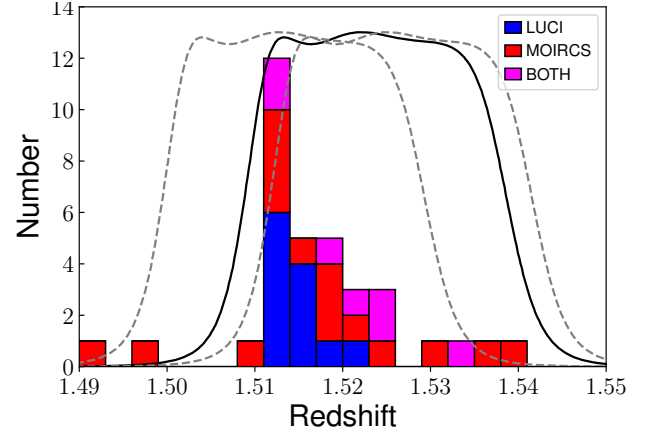


Figure 2. Redshift distribution of all our spectroscopic sample at $z_{\text{spec}} = 1.49 - 1.55$. The blue and red histograms show the number of galaxies observed with LBT/LUCI and Subaru/MOIRCS, respectively. Galaxies observed by both LUCI and MOIRCS are shown with the magenta histogram. The black- and grey-line curves represent the transmission curve of the MOIRCS narrow-band filter (NB1657) used in Koyama et al. (2014) at the center and the edge of the FoV, respectively (see Section 2).

stellar mass), but it is expected that the results would be biased to galaxies with larger H α flux. For example, since galaxies with large H α flux is expected to have pristine gas which have less oxygen in general, this may lead to an underestimate of the mean metallicity of our sample. Another possible way for the spectral stacking is to stack the spectra without normalization with H α flux (but putting a weight based on their background noise), but in this case, galaxies with strong H α emission (hence with high S/N) would largely contribute to the results. Because our aim is to study environmental dependence of the metallicity (determined by the H α /[N II] flux ratio) at fixed stellar mass, we decided to normalize the spectra based on the H α flux.

Finally, we stack the (normalized) spectra by calculating the mean flux density at each wavelength, weighted by the noise levels estimated in the original spectra (before normalization) because it represents the real quality of the spectra. We believe that the procedure described above is the best approach to study the mean H α /[N II] flux ratio in this study, but we verified that our conclusions are not changed even if we stack the spectra without any normalization. Fig. 4 shows our stacked spectra for each subsample.

We fit H α and [N II] $\lambda 6583$ lines of the stacked spectra with double Gaussian function (blue line in Fig. 4) with the peak flux density and the velocity width of H α and [N II] $\lambda 6583$ as free parameters (assuming the velocity widths are the same for H α and [N II] $\lambda 6583$). We

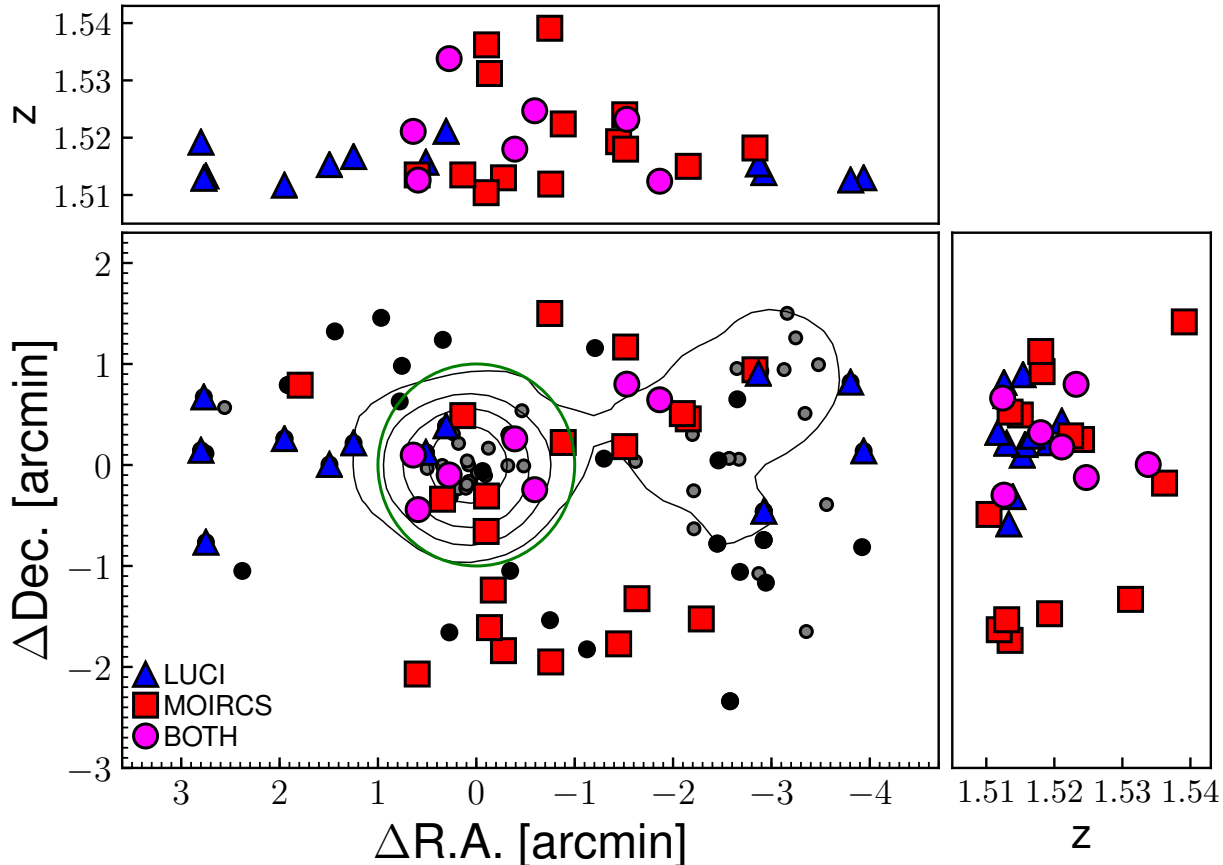


Figure 3. 2-D distribution of the cluster member galaxies in the 4C65.22 field. The grey dots represent all the photometric member galaxies identified in Koyama et al. (2014), while the black circles indicate our spectroscopic targets. The triangles, squares, and circles show galaxies of which $H\alpha$ line are detected with LBT/LUCI, Subaru/MOIRCS, and both, respectively. Galaxies within 1 arcmin from density peak (green circle) are used to determine the cluster redshift. The top and right panels show their projected distribution on the R.A.- z and Dec.- z plane, respectively. The black contours show the local density computed by using all the member galaxies from Koyama et al. (2014).

note that $[N II]\lambda 6548$ is also covered in the range of our spectroscopy, but we do not use it in our fitting process because of its low S/N ratio.

3.3. Mass-Metallicity Relation

The MZR is the correlation between galaxy stellar mass (M_*) and their oxygen abundance (e.g. Tremonti et al. 2004). In general, more massive galaxies tend to have higher metallicity, and the slope of the MZR becomes flatter in the massive end. Tremonti et al. (2004) suggested that the steepness of the MZR towards the low-mass end is related to the escape velocity of galactic outflow. Massive galaxies have deep potential well (hence require large escape velocity), which results in the decrease/suppression of outflowing gas; in other words, for more massive galaxies, a larger fraction of outflowing gas/material driven by their star forming activity returns to themselves. On the other hand, less massive galaxies have shallower potential well and require

smaller escape velocity. This scenario is consistent with the predictions of numerical simulations as well as some observational results (e.g. Finlator & Davé 2008; Davé et al. 2012; Erb et al. 2006; Onodera et al. 2016; Sanders et al. 2018). In addition, the gas fraction of galaxies is another important parameter which influences their gas-phase metallicity; i.e. gas-rich galaxies tend to have lower metallicity with higher star formation rate (e.g. Bothwell et al. (2013)).

In this paper, we investigate environmental impacts on the chemical enrichment in (star-forming) galaxies in cluster environment at $z = 1.52$. It should be noted that there are many metallicity calibrators used for distant galaxies. In this paper, we use the $[NII]/H\alpha$ method (Pettini & Pagel 2004) because of the limited wavelength coverage of our LUCI data. As we mentioned in the previous sections, we here use only 26 cluster member galaxies at $z = 1.52$ whose $H\alpha$ and $[N II]\lambda 6583$ are not contaminated by OH emission lines, in order to derive

the average $[\text{N II}]/\text{H}\alpha$ line flux ratio (see Sec.2.3; 3.2; Pettini & Pagel 2004).

We note that our sample is distributed over a wide stellar mass range. Some recent studies suggest that the environmental effect on MZR appears especially in the low-mass side (Kulas et al. 2013 and Shimakawa et al. 2015). To check this possibility, we divide our sample into the high- and low-mass subsamples based on their stellar mass (for LUCI and MOIRCS sample separately). Using the stacked spectrum of each subsample (see Fig.4), we calculate the N2 index, $N2 \equiv \log[\text{N II}]\lambda 6583/\text{H}\alpha$, for each stacked spectrum. We then derive their mean metallicity with the equation of $12 + \log(O/H) = 8.90 + 0.57 \times N2$ (Fig.5).

In Fig.5, we compare the average metallicity of our sample with the MZR for general field galaxies at the same redshifts. The grey shaded region shows the MZR for field galaxies at $1.4 < z < 1.7$ derived by Zahid et al. (2014), and the black solid line shows the result at $0.8 < z < 1.4$ derived by Stott et al. (2013), respectively. We note that the redshift range of the galaxy samples used in Stott et al. (2013) (313 at $z \sim 1.47$ and 68 at $z \sim 0.84$) is slightly different from that of our sample, but we believe that we can use their results as the comparison sample for our cluster galaxies at $z = 1.52$. In general, using a different method of metallicity calibration can produce different metallicity estimates. We here choose those two studies for our comparison, because they use the same metallicity calibration as our analysis (based on Pettini & Pagel 2004, N2 index) at similar redshifts. It can be seen that low-mass cluster galaxies ($10^{9.93}M_{\odot} < M_{*} < 10^{10.48}M_{\odot}$, blue symbols in Fig. 5) tend to be more metal rich than those in the field environment derived by Zahid et al. (2014), while the MZR at the same redshifts shown by Stott et al. (2013) is almost flat, which is in good agreement with our results. We expect that this difference between these two MZR for field galaxies is caused by the different sample selection. We will discuss more in detail about the potential bias in Sec.4.1.

4. DISCUSSION

With large efforts to investigate the metallicity of galaxies in the high- z Universe over the last decade, it is now established that the MZR exists in the high- z Universe (Erb et al. 2006; Maiolino et al. 2008; Troncoso et al. 2014; Onodera et al. 2016; Sanders et al. 2018), which is also reproduced by recent numerical simulations (Torrey et al. 2018). However, there are only countable studies on the environmental dependence of the MZR at high redshifts, and a consensus has yet to be reached on

the environmental impacts on the chemical enrichment within the galaxies.

Kulas et al. (2013) and Shimakawa et al. (2015) showed that low-mass (proto-)cluster galaxies tend to have *higher* metallicity than those in the field environment. They interpreted this trend as a result of a high metallicity recycling rate caused by cluster gaseous IGM with high pressure. On the other hand, Tran et al. (2015) and Kacprzak et al. (2015) showed that there is *no* environmental dependence in the MZR. Kacprzak et al. (2015) also used hydrodynamical simulations to show that the metallicity of galaxies in cluster and field environment are comparable. In contrast, Valentino et al. (2015) have investigated the MZR in a cluster at $z = 1.99$ and claimed that cluster galaxies have *lower* metallicity than those in the field environment. Their interpretation is that inflowing pristine gas would lower the gas metallicity within the galaxies and boost their SFR at the same time.

In this paper, we have focused on star-forming galaxies in a newly confirmed galaxy cluster around the radio galaxy, 4C65.22, at $z = 1.52$. With LUCI and MOIRCS spectroscopy presented in this paper, our results suggest that low-mass star-forming galaxies in the 4C65.22 field have slightly higher metallicity than those in Zahid et al. (2014) but comparable to Stott et al. (2013) (Fig.5). Below, we discuss which study is more appropriate for our comparison, and then we also discuss whether there is any environmental effect on the chemical enrichment in galaxies at this redshift.

4.1. Different Sample Selection

As shown in Fig.5, Stott et al. (2013) showed high metallicity in low-mass galaxies, implying a flat MZR, which is consistent with our results (black points and the connecting black line in Fig.5). On the other hand, MZR in Zahid et al. (2014) (grey shade in Fig.5) shows a clear difference from our results and Stott et al. (2013) in particular at the low-mass end ($10^{9.93}M_{\odot} < M_{*} < 10^{10.48}M_{\odot}$). We note that Stott et al. (2013) selected their targets primarily based on their NB $\text{H}\alpha$ imaging (HiZELS, $z = 0.84 - 1.47$; Sobral et al. 2013), while the targets in Zahid et al. (2014) are selected by the K-band magnitudes ($K < 23$ mag) and their broad-band colors.

Stott et al. (2013) explained that the reason of the discrepancy between their results and MZR shown by previous studies is the effect of dust attenuation in the photometric selection in the rest-UV and optical bands, which can miss dusty galaxies especially at low-mass side. Because dusty galaxies tend to have higher metallicity, Stott et al. (2013) claimed that the MZR in previous studies can be biased toward the low metal-

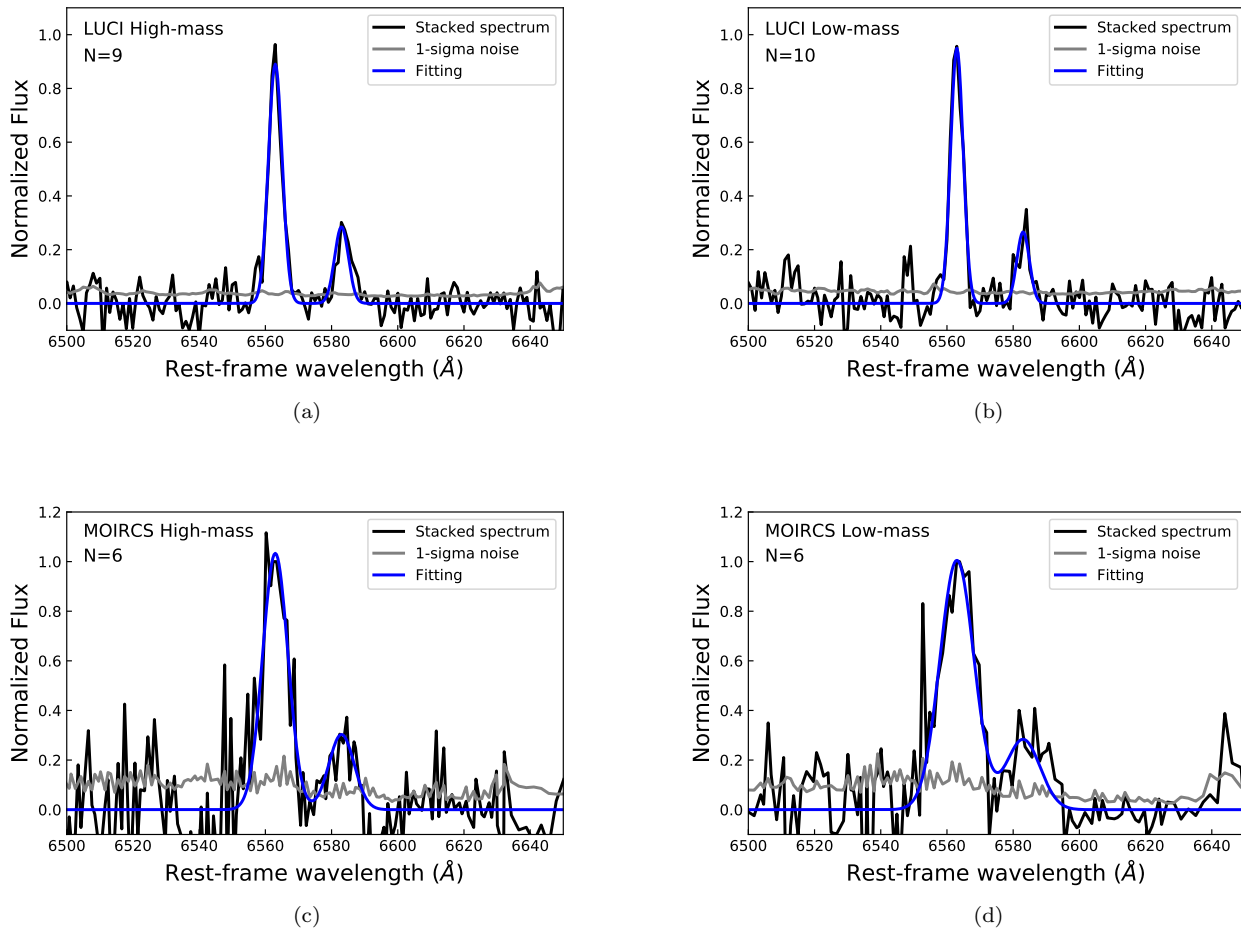


Figure 4. The 1-D stacked spectra of our cluster galaxies. The top panels show the stacked spectra for our LUCI sample, while the bottom panels show those of our MOIRCS sample. The left and right panels show the results for high-mass and low-mass bins, respectively. The black and grey lines show the stacked spectra and its 1-sigma error calculated from original data. The blue-line curve shows the best-fit double gaussian.

licity galaxies at the low-mass end. Also, Stott et al. (2013) point out that the samples in the previous studies are biased toward the higher SFR. In general, galaxies with higher SFR tend to show lower metallicity (so-called Fundamental Metallicity Relation; Mannucci et al. 2010), most likely driven by the increasing amount of pristine inflowing gas.

In order to avoid these biases, Zahid et al. (2014) selected their sample using K-band magnitude and color-color plane. Zahid et al. (2014) claimed that the effect of dust attenuation would move the object parallel to their criteria on the color-color diagram, so that their sample is not affected by the dust compared with UV-selected galaxies used in the previous studies (Daddi et al. 2004). They also argued that their exposure time for each target is much longer than that in Stott et al. (2013), which enables them to observe galaxies down to lower SFRs. For these reasons, Zahid et al. (2014) conclude that their

MZR and their suggestion on the redshift evolution of MZR should be valid.

Although the exact reason of the discrepancy between the results of these studies is unclear, we use the MZR of Stott et al. (2013) as the field sample compared with our results, because our original sample was selected with the narrow-band $H\alpha$ imaging survey performed by Koyama et al. (2014), i.e. the same method as Stott et al. (2013) for field galaxies. We note, however, that the choice of different field sample for the comparison can lead to a different interpretation on the environmental impacts on the MZR as shown in Fig.5.

4.2. Fundamental Metallicity Relation

Stott et al. (2013) fit the relation between the stellar mass, SFR, and the metallicity (Fundamental Metallicity Relation, FMR) of their sample at $z = 0.8 - 1.47$ using the 2-variable polynomial. The typical scatter

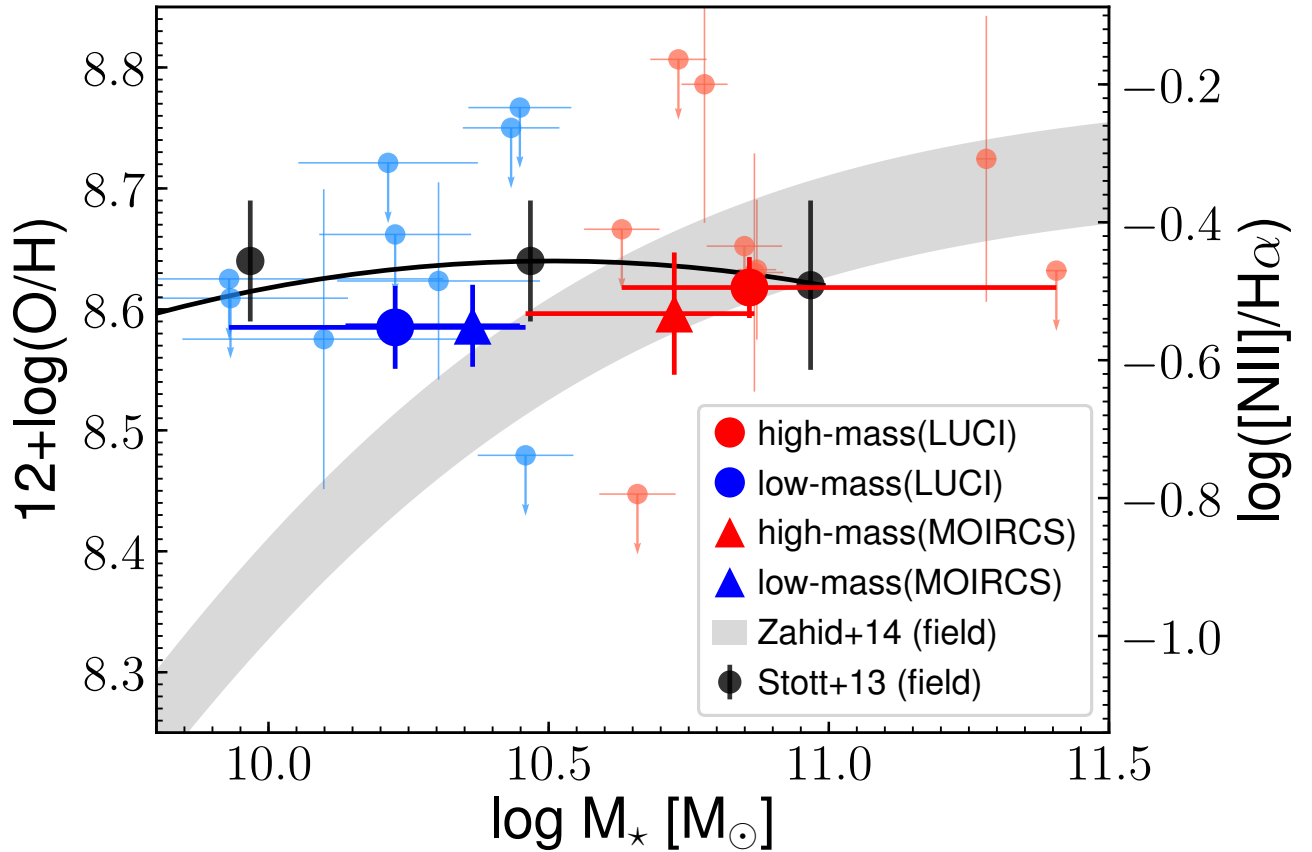


Figure 5. The MZR for our low-mass (blue) and high-mass (red) cluster sample at $z = 1.52$. The triangles and circles indicate the results for MOIRCS and LUCI sample, respectively. The stellar mass is the median of each subsample and horizontal error bar shows its bin size. Light blue and red points show the metallicity of individual galaxies observed with LUCI ($[N II] > 2\sigma$) and their upper limit ($[N II] < 2\sigma$). For comparison, we also show the MZR for field galaxies at $1.4 < z < 1.7$ from Zahid et al. (2014) (grey shade), and those at $0.8 < z < 1.4$ from Stott et al. (2013) (black solid line).

around the best-fit relation for their sample (σ) is 0.2 dex. This is about a factor of two smaller than the scatter around the fundamental plane reported for local galaxies (Mannucci et al. 2010). Stott et al. (2013) suggested the the FMR evolves with redshift, while the original work by Mannucci et al. (2010) suggested that the FMR does not change over the cosmic time.

In order to evaluate the environmental effects on the chemical enrichment in galaxies in the 4C65.22 cluster field, we here calculate the metallicity offset from the FMR of Stott et al. (2013), $\Delta[12 + \log(O/H)] = (12 + \log(O/H))_{obs} - (12 + \log(O/H))_{S13}$, and the results are shown in Fig.6.

We find that both low- and high-mass MOIRCS subsamples and the low-mass LUCI sample show $\Delta[12 + \log(O/H)] < 1\sigma$. The LUCI high-mass sample shows slightly larger deviation from the FMR of Stott et al. (2013), but it is still within 2σ level. Therefore, we consider that our sample has similar properties in their gas-

phase metallicity to the field galaxies at similar redshifts. This can be interpreted as that the balance between the inflow and outflow in the dense environment would not be affected by global environment.

5. SUMMARY

We present the results of our NIR spectroscopic observations with LUCI and MOIRCS of 71 star-forming galaxies in a high-redshift ($z = 1.52$) galaxy cluster candidate discovered by Koyama et al. (2014). We successfully determined the spectroscopic redshifts of 39 galaxies with $H\alpha$ and $[O III]\lambda 5007$ lines. We confirm the redshift of the central region in this cluster to be $z = 1.517$ (< 500 kpc from the peak of galaxy overdensity) and confirm that this is a real, physically associated, well-matured cluster at $z = 1.517$. By mapping the 3-D structures around the cluster, we find a hint that this cluster is located at the intersection of two filaments/sheet-like structures, and the large-scale

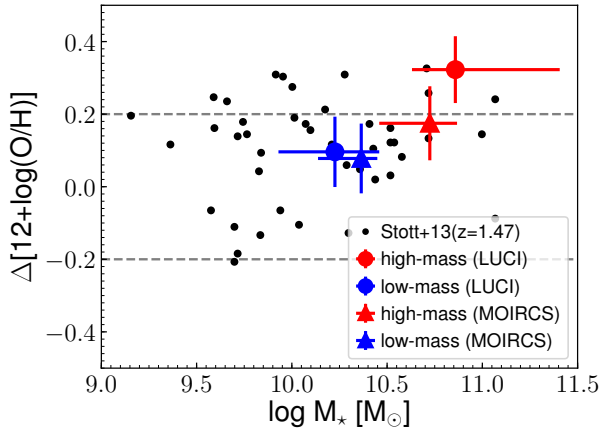


Figure 6. The offset from the fundamental plane established by Stott et al. (2013) (in the metallicity direction) against the stellar mass for our cluster sample (colored symbols; the meanings of the symbols are the same as Fig.5). The black points are the HiZELS-FMOS sample at $z = 1.47$ from Stott et al. (2013). Both high- and low-mass samples of our MOIRCS data, as well as the low-mass sample for our LUCI data, are located within the 1σ (0.2 dex, grey dashed lines) from the field FMR. The high-mass sample of LUCI data shows slightly larger offset, but it is still within $<2\sigma$ level.

structures may be extended even beyond our survey field.

We then divide our spectroscopic members of this cluster environment into two subsamples by the median of their stellar mass, at $10^{10.48} M_{\odot}$ (for those observed with LUCI and MOIRCS separately). For each subsample, we performed stacking analysis after subtracting continuum and normalizing each spectrum by their $H\alpha$ flux. We derived "mean" metallicity of each subsample without being affected by those with very strong OH sky lines. Using these stacked spectra and the commonly used N2 method developed by Pettini & Pagel (2004), we investigated the environmental dependence of gas-phase metallicity in galaxies at $z \sim 1.5$. We note that our sample would not be strongly affected by type-1 AGNs, but we cannot rule out the possibility of some contamination from type-2 AGNs with the current data alone.

By comparing the MZR of our cluster sample to that of field galaxies at similar redshifts derived by Stott et al. (2013), we find that the metallicity of our targets is consistent with the field galaxies. On the other hand, the metallicity of our less massive galaxies ($10^{9.93} M_{\odot} < M_* < 10^{10.48} M_{\odot}$) shows a slight enhancement from the MZR of Zahid et al. (2014). Importantly, our targets and the sample in Stott et al. (2013) are selected by NB ($H\alpha$) selection, while Zahid et al. (2014) select their

sample by the K-band magnitude. The discrepancy between the two studies for field galaxies could be caused by their different sample selection, and thus we consider that it would be more appropriate to compare our results to Stott et al. (2013), who selected their spectroscopic sample from the NB ($H\alpha$) imaging data.

We then investigated the metallicity offset of our cluster sample from the FMR shown by Stott et al. (2013). We find that both of our MOIRCS subsamples and the LUCI low-mass sample are consistent with the FMR of Stott et al. (2013) within 1σ . The LUCI high-mass sample shows a slightly larger offset, but it is still within 2σ level. We therefore conclude that our cluster galaxies have the gas-phase metallicity comparable to the field galaxies at similar redshifts.

It should be noted that some previous studies show a lower, consistent, and higher metallicity in high- z clusters compared to field galaxies (e.g. Kulas et al. 2013, Shimakawa et al. 2015, Valentino et al. 2015, Tran et al. 2015, Kacprzak et al. 2015). The authors always try to introduce some preferable mechanisms to explain their results; e.g. higher recycling rate, enriched IGM, and pristine inflow, all of which are supported by the observations or simulations (e.g. Davé et al. 2008, Davé et al. 2011, Dekel et al. 2009, Ellison et al. 2013, Torrey et al. 2012). Continuous efforts for determining the MZR in high- z cluster environments are necessary to understand whether environment would ubiquitously affect the galaxy metallicity and, if the environment really matters, we need to understand what kind of process is at work.

ACKNOWLEDGEMENT

We thank the referee for reviewing our paper and providing us with useful comments which improved the paper. This work was financially supported in part by a Grant-in-Aid for the Scientific Research (Nos. JP17K14257; 18K13588) by the Japanese Ministry of Education, Culture, Sports and Science. This paper is based on data collected at Subaru Telescope, which is operated by the National Astronomical Observatory of Japan, as well as by observations made with the Large Binocular Telescope, which is an international collaboration among institutions in the United States, Italy and Germany. LBT Corporation partners are: LBT Beteiligungsgesellschaft, Germany, representing the Max-Planck Society, the Astrophysical Institute Potsdam, and Heidelberg University; The University of Arizona on behalf of the Arizona university system; Istituto Nazionale di Astrofisica, Italy; The Ohio State University, and The Research Corporation, on behalf of

The University of Notre Dame, University of Minnesota
and University of Virginia.

REFERENCES

- Andrews, B. H., & Martini, P. 2013, *ApJ*, 765, 140
- Baldwin, J. A., Phillips, M. M., & Terlevich, R. 1981, *PASP*, 93, 5
- Balogh, M., Eke, V., Miller, C., et al. 2004, *MNRAS*, 348, 1355
- Bothwell, M. S., Maiolino, R., Kennicutt, R., et al. 2013, *MNRAS*, 433, 1425
- Brinchmann, J., Charlot, S., White, S. D. M., et al. 2004, *MNRAS*, 351, 1151
- Buat, V. 2003, *SF2A-2003: Semaine de l’Astrophysique Francaise*, 235
- Butcher, H., & Oemler, A., Jr. 1984, *ApJ*, 285, 426
- Cooper, M. C., Tremonti, C. A., Newman, J. A., & Zabludoff, A. I. 2008, *MNRAS*, 390, 245
- Daddi, E., Cimatti, A., Renzini, A., et al. 2004, *ApJ*, 617, 746
- Davé, R., Oppenheimer, B. D., & Sivanandam, S. 2008, *MNRAS*, 391, 110
- Davé, R., Finlator, K., & Oppenheimer, B. D. 2011, *MNRAS*, 416, 1354
- Davé, R., Finlator, K., & Oppenheimer, B. D. 2012, *MNRAS*, 421, 98
- Dekel, A., Sari, R., & Ceverino, D. 2009, *ApJ*, 703, 785
- Dressler, A. 1980, *ApJ*, 236, 351
- Ellison, S. L., Patton, D. R., Simard, L., & McConnachie, A. W. 2008, *ApJL*, 672, L107
- Ellison, S. L., Mendel, J. T., Patton, D. R., & Scudder, J. M. 2013, *MNRAS*, 435, 3627
- Erb, D. K., Shapley, A. E., Pettini, M., et al. 2006, *ApJ*, 644, 813
- Finlator, K., & Davé, R. 2008, *MNRAS*, 385, 2181
- Genzel, R., Förster Schreiber, N. M., Rosario, D., et al. 2014, *ApJ*, 796, 7
- Goto, T., Yamauchi, C., Fujita, Y., et al. 2003, *MNRAS*, 346, 601
- Gupta, A., Yuan, T., Torrey, P., et al. 2018, *MNRAS*, 477, L35
- Gómez, P. L., Nichol, R. C., Miller, C. J., et al. 2003, *ApJ*, 584, 210
- Hopkins, A. M., & Beacom, J. F. 2006, *ApJ*, 651, 142
- Ichikawa, T., Suzuki, R., Tokoku, C., et al. 2006, *Proc. SPIE*, 6269, 626916
- Kacprzak, G. G., Yuan, T., Nanayakkara, T., et al. 2015, *ApJL*, 802, L26
- Kewley, L. J., Maier, C., Yabe, K., et al. 2013, *ApJ*, 774, L10.
- Kobayashi, C. 2007, *EAS Publications Series*, 24, 245
- Koyama, Y., Smail, I., Kurk, J., et al. 2013, *MNRAS*, 434, 423
- Koyama, Y., Kodama, T., Tadaki, K.-i., et al. 2014, *ApJ*, 789, 18
- Koyama, Y., Kodama, T., Hayashi, M., et al. 2015, *MNRAS*, 453, 879
- Kulas, K. R., McLean, I. S., Shapley, A. E., et al. 2013, *ApJ*, 774, 130
- Li, I. H., Glazebrook, K., Gilbank, D., et al. 2011, *MNRAS*, 411, 1869
- Maier, C., Hayashi, M., Ziegler, B. L., et al. 2019, *arXiv e-prints*, arXiv:1903.09591.
- Maiolino, R., Nagao, T., Grazian, A., et al. 2008, *A&A*, 488, 463
- Mannucci, F., Cresci, G., Maiolino, R., Marconi, A., & Gnerucci, A. 2010, *MNRAS*, 408, 2115
- Miyazaki, S., Komiyama, Y., Sekiguchi, M., et al. 2002, *PASJ*, 54, 833
- Onodera, M., Carollo, C. M., Lilly, S., et al. 2016, *ApJ*, 822, 42
- Peng, Y.-j., Lilly, S. J., Kovač, K., et al. 2010, *ApJ*, 721, 193
- Pettini, M., & Pagel, B. E. J. 2004, *MNRAS*, 348, L59
- Salmon, B., Papovich, C., Finkelstein, S. L., et al. 2015, *ApJ*, 799, 183
- Salpeter, E. E. 1955, *ApJ*, 121, 161
- Sanders, R. L., Shapley, A. E., Kriek, M., et al. 2018, *ApJ*, 858, 99
- Santini, P., Fontana, A., Castellano, M., et al. 2017, *ApJ*, 847, 76
- Seifert, W., Appenzeller, I., Baumeister, H., et al. 2003, *Proc. SPIE*, 4841, 962
- Shimakawa, R., Kodama, T., Tadaki, K.-i., et al. 2015, *MNRAS*, 448, 666
- Sobral, D., Best, P. N., Matsuda, Y., et al. 2012, *MNRAS*, 420, 1926
- Sobral, D., Smail, I., Best, P. N., et al. 2013, *MNRAS*, 428, 1128
- Stott, J. P., Sobral, D., Bower, R., et al. 2013, *MNRAS*, 436, 1130
- Suzuki, R., Tokoku, C., Ichikawa, T., et al. 2008, *PASJ*, 60, 1347

- Tadaki, K.-i., Kodama, T., Tanaka, I., et al. 2013, *ApJ*, 778, 114
- Tanaka, M., Goto, T., Okamura, S., Shimasaku, K., & Brinkmann, J. 2004, *AJ*, 128, 2677
- Tanaka, I., De Breuck, C., Kurk, J. D., et al. 2011, *PASJ*, 63, 415
- Tomczak, A. R., Quadri, R. F., Tran, K.-V. H., et al. 2016, *ApJ*, 817, 118
- Torrey, P., Cox, T. J., Kewley, L., & Hernquist, L. 2012, *ApJ*, 746, 108
- Torrey, P., Vogelsberger, M., Hernquist, L., et al. 2018, *MNRAS*, 477, L16
- Tran, K.-V. H., Nanayakkara, T., Yuan, T., et al. 2015, *ApJ*, 811, 28
- Tremonti, C. A., Heckman, T. M., Kauffmann, G., et al. 2004, *ApJ*, 613, 898
- Troncoso, P., Maiolino, R., Sommariva, V., et al. 2014, *A&A*, 563, A58
- Valentino, F., Daddi, E., Strazzullo, V., et al. 2015, *ApJ*, 801, 132
- Vulcani, B., Poggianti, B. M., Finn, R. A., et al. 2010, *ApJL*, 710, L1
- Wu, P.-F., Zahid, H. J., Hwang, H. S., & Geller, M. J. 2017, *MNRAS*, 468, 1881
- York, D. G., Adelman, J., Anderson, J. E., Jr., et al. 2000, *AJ*, 120, 1579
- Yoshikawa, T., Akiyama, M., Kajisawa, M., et al. 2010, *ApJ*, 718, 112
- Zahid, H. J., Kashino, D., Silverman, J. D., et al. 2014, *ApJ*, 792, 75
- van Dokkum, P. G., Franx, M., Fabricant, D., Illingworth, G. D., & Kelson, D. D. 2000, *ApJ*, 541, 95
- Villar, V., Gallego, J., Pérez-González, P. G., et al. 2008, *ApJ*, 677, 169
- Whitaker, K. E., Franx, M., Leja, J., et al. 2014, *ApJ*, 795, 104